

ACTIVA: Amortized Causal Effect Estimation via Transformer-based Variational Autoencoder

Andreas Sauter¹, Saber Salehkaleybar², Aske Plaat², Erman Acar³

¹Vrije Universiteit Amsterdam

²LIACS Leiden University

³IvI and ILLC, Universiteit van Amsterdam

The Netherlands

a.sauter@vu.nl

Abstract

Predicting the distribution of outcomes under hypothetical interventions is crucial across healthcare, economics, and policy-making. However, existing methods often require restrictive assumptions, and are typically limited by the lack of amortization across problem instances. We propose ACTIVA, a transformer-based conditional variational autoencoder (VAE) architecture for amortized causal inference, which estimates interventional distributions directly from observational data without. ACTIVA learns a latent representation conditioned on observational inputs and intervention queries, enabling zero-shot inference by amortizing causal knowledge from diverse training scenarios. We provide theoretical insights showing that ACTIVA predicts interventional distributions as mixtures over observationally equivalent causal models. Empirical evaluations on synthetic and semi-synthetic datasets confirm the effectiveness of our amortized approach and highlight promising directions for future real-world applications.

1 Introduction

Understanding the causal effects of an action by pure observation is central in many domains including healthcare (Shi and Norgeot 2022), economics (Panizza and Presbitero 2014), and finance (Kumar et al. 2023). Yet, estimating these effects is constraint by inherent limitations regarding the conclusions that can be drawn from observations only (Bareinboim et al. 2022). Specifically, looking only at observational data leads to ambiguities over which causal effect a certain action will have.

To address these ambiguities, current approaches to causal inference often rely on strong assumptions (see 7 for more detail). An alternative road to deal with these ambiguities is to make them explicit in the form of uncertainties. For example providing a interval or distribution of plausible causal effects has been shown to be feasible and useful in practice (Maathuis et al. 2009; Balazadeh et al. 2025). Such a prediction allows for a clearer picture on what effects to expect and can lead to actionable inferences if e.g. the range of effects lies within an interval that leads to the same actions.

Although having a distribution over causal effects is a promising direction, it only represents uncertainty over this specific point-estimate. A natural extension of this is to look at the overall distribution shift of the causal factors af-

ter performing an action. Additionally to answering cause-effect questions, such a distribution can provide further task-relevant insights such as multimodality and hence prevent erroneous average effect predictions.

Recent work further emphasizes the reuse of learned knowledge of diverse causal tasks across different queries to improve inference efficiency by learning one model for estimation of different problem instances (Löwe et al. 2022; Lorch et al. 2022; Scetbon et al. 2024; Sauter et al. 2024; Mahajan et al. 2024; Annadani et al. 2025; Robertson et al. 2025; Balazadeh et al. 2025; Ma et al. 2025). Results from these approaches suggest that we can effectively amortize over datasets coming from different causal models for various downstream tasks.

In this paper, we address above restrictions by proposing a causal encoder-decoder architecture called ACTIVA. During training, the encoder maps the interventional data to a latent space conditioned on observational data and an interventional query, and the decoder transforms the encoded causal information into interventional distribution. At inference time, we condition our prior on the observational data alone to obtain a distribution over plausible causal models which the decoder transforms into a mixture over these models. We provide a theoretical analysis on the specific nature of our latent and decoded space. In empirical evaluations, we show that our architecture can successfully recover causal information at inference time even on novel instances. This allows for the potential zero-shot transfer from simulated scenarios to the real-world ones without knowing the causal relations neither during, avoiding common pitfalls when relying on such graphs (Poinsot et al. 2024). Below we provide a detailed list of our main contributions:

- We provide a conditional variational autoencoder model (ACTIVA) designed for amortized causal distribution shift estimation. Our model takes an observational dataset and a query intervention as input, predicts a latent representation of the dataset and outputs an estimate of the respective interventional distribution.
- We analyze the proposed model theoretically, leading to rare fundamental insights about amortized causal inference. The result emphasizes that amortized causal inference is inherently limited by identifiability from the data. Nevertheless it can recover shift distributions up to a mixture of shifts from observationally equivalent models.

- We implement an instantiation of ACTIVA and show empirically that it predicts interventional distributions given observational data and interventional queries both on synthetic and semi-synthetic data.

Overall, our work highlights the significance of amortized causal inference as a tool to overcome traditional hurdles in distributional causal effect estimation.¹

2 Background and Notation

Next, we introduce the notation and the formal details for β -VAEs and causality.

2.1 Conditional β -VAEs

Variational Autoencoders (VAEs) are generative models that approximate the joint distribution $p_\theta(\mathbf{x}, \mathbf{z}) = p_\gamma(\mathbf{x}|\mathbf{z})p_\eta(\mathbf{z})$, where \mathbf{z} are latent variables governing the data \mathbf{x} and $\theta = \{\gamma, \eta\}$ are the parameters determining the data generation. The marginal data likelihood $p_\theta(\mathbf{x})$ is optimized using the evidence lower bound (ELBO) (Kingma and Welling 2013):

$$\log p_\theta(\mathbf{x}) \geq \mathbb{E}_{q_\phi(\mathbf{z}|\mathbf{x})} [\log p_\gamma(\mathbf{x}|\mathbf{z})] - \text{KL}(q_\phi(\mathbf{z}|\mathbf{x})\|p_\eta(\mathbf{z})). \quad (1)$$

Where ϕ parametrizes the encoding distribution q . The ELBO has a reconstruction term, which ensures the model accurately reconstructs the data from the latent representation, and a Kullback-Leibler divergence (KL) term, which regularizes the encoding distribution $q_\phi(\mathbf{z}|\mathbf{x})$ to approximate some prior $p_\eta(\mathbf{z})$.

Conditional VAEs (CVAEs) (Sohn, Yan, and Lee 2015) extend this framework to allow for conditional generation with some auxiliary information \mathbf{c} . The generative process of CVAEs follows a conditional prior such that

$$p_\theta(\mathbf{x}, \mathbf{z}|\mathbf{c}) = p_\gamma(\mathbf{x}|\mathbf{z}, \mathbf{c})p_\eta(\mathbf{z}|\mathbf{c}). \quad (2)$$

In β -VAEs (Higgins et al. 2017), the KL term is scaled by a hyperparameter β , leading to a modified ELBO as follows:

$$\mathbb{E}_{q_\phi(\mathbf{z}|\mathbf{x}, \mathbf{c})} [\log p_\gamma(\mathbf{x}|\mathbf{z}, \mathbf{c})] - \beta \text{KL}(q_\phi(\mathbf{z}|\mathbf{x}, \mathbf{c})\|p_\eta(\mathbf{z}|\mathbf{c})). \quad (3)$$

The choice of β governs the trade-off between accurately reconstructing the data and disentangling the latent representations. While $\beta > 1$ emphasizes disentanglement, in our setting, we use $\beta < 1$ to prioritize accurate reconstruction.

2.2 Causal Models

In this paper, we employ the notation of structural causal models (SCM) for describing causal data generating processes. For a detailed definition, we refer the reader to (Bareinboim et al. 2022).

We treat a causal model \mathcal{M} as a generative process over d variables $\mathbf{V} = \{V_1, \dots, V_d\}$, denoting an assignment of these variables as $\mathbf{v} = \{v_1, \dots, v_d\}$. The model is causal in the sense that each variable is the direct cause of a subset of

¹The code to our model is available at https://anonymous.4open.science/r/Amortized_Interventional_Distribution_Estimation-E182/

V . Specifically, any variable $V_j \in \mathbf{V}$ is determined by its direct causes with $V_j \leftarrow f_j(Pa_{V_j}, U_j)$, where f_j is an arbitrary function of the direct causes Pa_{V_j} (representing parent variables of V_j) and a noise term U_j . We call two models equivalent if all their parameters are equal. All causal relations combined form the causal graph $G^{\mathcal{M}}$. Each model \mathcal{M} induces a joint distribution $p_{\mathcal{M}}(\mathbf{V})$, called the observational distribution. All models with the same observational distribution form a so-called Markov equivalence class (MEC).

In a causal model, performing a so-called intervention $do(V = v)$, manipulates \mathcal{M} such that the target variable V is forced to take on value v , regardless of V 's causes. Such an intervention results in an intervened model that we denote $\mathcal{M}_{do(V=v)}$ or $\mathcal{M}_{do(V)}$ when v is clear from the context. We denote the variables of $\mathcal{M}_{do(V=v)}$ as $\mathbf{V} \mid do(V = v)$. In this work, v is one possible intervention value for which the training data contains samples. Similarly to its observational counterpart, $\mathcal{M}_{do(V)}$ induces a joint distribution $p_{\mathcal{M}}(\mathbf{V} \mid do(V))$ that we call the interventional distribution.

The aim of this work is to estimate the causally shifted distribution $p_{\mathcal{M}}(\mathbf{V} \mid do(V))$ from an observational dataset $\mathbf{D}^{\mathcal{M}} = \mathbf{v}_{1:N}^{\mathcal{M}}$, where N is the number of i.i.d. samples and $\mathbf{v}_n^{\mathcal{M}} \sim p_{\mathcal{M}}(\mathbf{V})$. In general, identifying this distribution is not possible without additional assumptions or interventional data because of the ambiguities introduced by MECs (Bareinboim et al. 2022). This fundamental property of causality naturally extends to our work which we address in the theoretical portion of this work on data with identifiable effects.

3 ACTIVA

In this section, we outline a β -CVAE architecture for amortized causal distribution shift estimation called ACTIVA. In our setup, a dataset of observational samples and a query intervention serve as a conditional for the following generative process:

$$p_\theta(\mathbf{V}, \mathbf{z} \mid \mathbf{D}^{\mathcal{M}}, do(V)) = p_\gamma(\mathbf{V} \mid \mathbf{z})p_\eta(\mathbf{z} \mid \mathbf{D}^{\mathcal{M}}, do(V)) \quad (4)$$

Intuitively, the data is modeled by a conditional prior that maps the observational data $\mathbf{D}^{\mathcal{M}}$ and query intervention $do(V)$ to a latent code \mathbf{z} . The latents then contain all information the model needs to reconstruct the data; in our case the samples from a post-interventional distribution \mathbf{V} .

To find parameters θ , we use the conditional ELBO formulation for likelihood maximization as in (3). Translated to our model, our overall learning objective becomes:

$$\begin{aligned} \mathcal{L}(\theta, \phi) = & \mathbb{E}_{q_\phi(\mathbf{z} \mid \mathbf{V}, \mathbf{D}^{\mathcal{M}}, do(V))} [\log p_\gamma(\mathbf{V} \mid \mathbf{z})] \\ & - \text{KL}(q_\phi(\mathbf{z} \mid \mathbf{V}, \mathbf{D}^{\mathcal{M}}, do(V)) \parallel p_\eta(\mathbf{z} \mid \mathbf{D}^{\mathcal{M}}, do(V))), \end{aligned} \quad (5)$$

where $q_\phi(\mathbf{z} \mid \mathbf{V}, \mathbf{D}^{\mathcal{M}}, do(V))$ is the encoding distribution, $p_\gamma(\mathbf{V} \mid \mathbf{z})$ the decoder distribution, and $p_\eta(\mathbf{z} \mid \mathbf{D}^{\mathcal{M}}, do(V))$ the conditional prior.

To estimate the objective from data, we assume to have training data $\mathbf{D}^{tr} = [\mathbf{v}_n^{\mathcal{M}_{do(V)}}, \mathbf{D}^{\mathcal{M}}, do(V)]_{j=0}^J$ with J

training examples pairing interventional samples with observational ones and the corresponding intervention. Where $\mathbf{D}_j^{tr} \sim p_{tr}(\mathbf{D}^{tr}) = \int p_{tr}(\mathbf{D}^{tr} \mid \mathcal{M}) p_{tr}(\mathcal{M}) d\mathcal{M}$ is an element from the training data distribution according to a pre-defined distributions of causal models $p_{tr}(\mathcal{M})$. This pre-defined distribution can be seen as the simulator that models causal models that we expect at inference time.

To enable gradient-based optimization, we use the reparameterization trick (Kingma and Welling 2013), allowing backpropagation through the stochastic sampling process of q_ϕ . For our final objective, we aim at amortizing prediction over the training distribution of causal model, to successfully apply our model to data sets that were not in the training data. Optimizing our amortized objective then amounts to minimizing the expectation of our loss regarding the distribution of the training datasets.

$$\min_{\theta, \phi} \mathbb{E}_{\mathbf{D}_j^{tr} \sim p_{tr}(\mathbf{D}^{tr})} \mathcal{L}(\theta, \phi) \quad (6)$$

This objective ensures that our model can make inferences on datasets coming from the class of predefined causal models, even if the specific dataset was not in the training set. It furthermore implies that the more general the training distribution of data sets is, the more the model will generalize to new data sets during inference as has also been argued in (Montagna et al. 2024).

4 Theoretical Analysis

In this section, we show that inference with the model specified above gives us a mixture of all causal shift distributions that are consistent with the observational data. We start with two assumptions.

Assumption 1: $q_\phi(\mathbf{z}|\mathbf{V}, \mathbf{D}^{\mathcal{M}}, do(V))$ correctly identifies the causal model, i.e., $q_\phi(\mathbf{z}|\mathbf{V}, \mathbf{D}^{\mathcal{M}}, do(V)) = q_\phi(\mathbf{z}|\mathbf{V}, \mathbf{D}^{\mathcal{M}'}, do(V)) \Rightarrow \mathcal{M} = \mathcal{M}'$.

This assumption implies that the models in the training data \mathbf{D}^{tr} must be identifiable from the observational and interventional data. Furthermore, we assume

Assumption 2: The decoder is injective, i.e., for two inputs $\mathbf{z} \neq \mathbf{z}' \Rightarrow dec_\gamma(\mathbf{z}) \neq dec_\gamma(\mathbf{z}') \Rightarrow p_\gamma(\mathbf{V}|\mathbf{z}) \neq p_\gamma(\mathbf{V}|\mathbf{z}')$.

Next, we show that the encoder distribution must place all probability mass on a single point.

Definition 1 (Dirac distribution, informal): Let the Dirac distribution be defined via its density as $\delta_{z_k}(x) = \begin{cases} \infty & \text{if } x = z_k \\ 0 & \text{otherwise} \end{cases}$ such that $\int_{-\infty}^{\infty} \delta_{z_k}(x) dx = 1$. Such distribution places all probability on one point.

Lemma 1: Under Assumptions 1-2, $q_\phi(\mathbf{z}|\mathbf{V}, \mathbf{D}^{\mathcal{M}}, do(V))$ is a Dirac distribution.

Proof: Take any two equivalent models $\mathcal{M} = \mathcal{M}'$ and two samples $\mathbf{z} \sim q_\phi(\mathbf{z}|\mathbf{V}, \mathbf{D}^{\mathcal{M}}, do(V))$, $\mathbf{z}' \sim q_\phi(\mathbf{z}|\mathbf{V}, \mathbf{D}^{\mathcal{M}'}, do(V))$. Suppose that the two samples differ, i.e. $\mathbf{z} \neq \mathbf{z}'$, then we know from Assumption 2 that

$p_\gamma(\mathbf{V}|\mathbf{z}) \neq p_\gamma(\mathbf{V}|\mathbf{z}')$. But since we know that they represent the same model (Assumption 1), the two resulting distributions over \mathbf{V} must be the same, which leads to a contradiction. Therefore, \mathbf{z} and \mathbf{z}' must be the same. Accordingly, $q_\phi(\mathbf{z}|\mathbf{V}, \mathbf{D}^{\mathcal{M}}, do(V))$ must always yield the same sample, and the proof is complete.

Note that taking Lemma 1 and Assumption 1 together let's us interpret z_k as the latent representation of the causal model \mathcal{M}^k and intervention query.

Next, we investigate what the learned prior will look like under the above assumptions. This will help us to further investigate the estimated interventional distribution.

Note that for the amortized loss in (6), we can rearrange the loss computation as follows by sorting the training samples accordingly: $\frac{1}{J} \sum_{\mathbf{D}^{tr}} \mathcal{L} = \frac{1}{J} \sum_I \sum_O \sum_{\mathbf{D}_{[\mathcal{M}^o]}^{tr}} \mathcal{L}$, where J is the number of datapoints, I is the set of possible interventions, O is a partition over the datasets according to their Markov equivalence class and $\mathbf{D}_{[\mathcal{M}^o]}^{tr}$ is the set of training examples within the equivalence class with representative \mathcal{M}^o , s.t. $\mathbf{D}_{[\mathcal{M}^o]}^{tr} = \{[\mathbf{v}_n^{\mathcal{M}_{do(V)}}, \mathbf{D}^{\mathcal{M}}]_j \in \mathbf{D}^{tr} : p_{\mathcal{M}}(\mathbf{D}^{\mathcal{M}}) = p_{\mathcal{M}^o}(\mathbf{D}^{\mathcal{M}^o})\}$. In other words, $\mathbf{D}_{[\mathcal{M}^o]}^{tr}$ contains all data-points where the probability of generating such observational data-points by \mathcal{M} is the same as the one by \mathcal{M}^o .

This decomposition is necessary to derive the alternative form of the ELBO according to (Hoffman and Johnson 2016) as described next. We define in the following $\bar{q}_\phi(\mathbf{z}|\mathbf{D}_{[\mathcal{M}^o]}^{tr}, do(V)) := \frac{1}{J} \sum_{\mathbf{D}_j^{tr}} q_\phi(\mathbf{z}|\mathbf{D}_j^{tr})$ which is a uniform mixture of Dirac distributions as per Lemma 1 with $\pi_c = \frac{1}{J}$ for all component weights π_c by construction. In other words, \bar{q}_ϕ is the distribution that averages over all encoder distributions that identify models that are observationally equivalent to \mathcal{M}^o . Treating the sample index j as random variable, we can further define $q(j, \mathbf{z}) := \frac{1}{J} q(\mathbf{z}|\mathbf{D}_j^{tr})$. Finally, this allows us to decompose the KL term in our loss into

$$\begin{aligned} & \frac{1}{J} \sum_{\mathbf{D}_j^{tr}} \text{KL}(q_\phi(\mathbf{z}|\mathbf{D}_j^{tr}) \parallel p_\eta(\mathbf{z}|\mathbf{D}^{\mathcal{M}}, do(V))_j) \\ &= \text{KL}(\bar{q}_\phi(\mathbf{z}|\mathbf{D}_{[\mathcal{M}^o]}^{tr}, do(V)) \parallel p_\eta(\mathbf{z}|\mathbf{D}^{\mathcal{M}}, do(V))_o) \\ & \quad + \mathbb{I}_{q(j, \mathbf{z})}[j, \mathbf{z}], \end{aligned} \quad (7)$$

where $\mathbb{I}_{q(j, \mathbf{z})}[j, \mathbf{z}]$ is the mutual information.

Since the resulting KL term is the only term that involves the prior, we focus our further analysis only on that term and disregard the mutual information. To ensure the KL is well-defined, we additionally make the following assumption.

Assumption 3: The prior is a finite mixture of Dirac distributions which has zero mass, where \bar{q}_ϕ has zero mass, i.e., $p_\eta(\mathbf{z}|\mathbf{D}^{\mathcal{M}}, do(V)) = \sum_C \rho_c \delta_{\mathbf{z}_c}(\mathbf{z})$ s.t. $\forall \mathbf{z}_c : \bar{q}_\phi(\mathbf{z}_c|\mathbf{D}^{[\mathcal{M}^o]}, do(V)) = 0 \Rightarrow p_\eta(\mathbf{z}_c|\mathbf{D}^{\mathcal{M}}, do(V)) = 0$.

Intuitively, this implies that we have prior knowledge on which models do not fall into the observational equivalence class of the input dataset.

Proposition 1: The prior $p_\eta(\mathbf{z}|\mathbf{D}^{\mathcal{M}}, do(V))_o$ becomes equal to $\bar{q}_\phi(\mathbf{z}|\mathbf{D}_{[\mathcal{M}^o]}^{tr}, do(V)) \forall o \in O$ when the ELBO is

minimized.

Proof: As argued above, the only term in our affecting p_η is the KL term in (7) which needs to become zero to be minimized for each o . As per Assumption 3 and the definition of \bar{q}_ϕ , this term becomes $\sum_C \pi_c \log \frac{\pi_c}{\rho_c}$ which is 0 exactly when $\forall c : \pi_c = \rho_c = \frac{1}{J}$. Hence, $p_\eta(\mathbf{z} | [\mathbf{D}^{\mathcal{M}}, do(V)]_o) = \bar{q}_\phi(\mathbf{z} | \mathbf{D}_{[\mathcal{M}^o]}^{tr}, do(V))$ when (6) is minimized.

Lastly, we show that our method recovers a mixture of post-interventional distributions consistent with the observational data.

Proposition 2: The conditional generative distribution $p_\theta(\mathbf{V} | [\mathbf{D}^{\mathcal{M}}, do(V)]_j)$ is a mixture of distributions $\sum_{\mathcal{M}^k \in [\mathcal{M}^j]} \rho_k p(\mathbf{V} | \mathbf{D}^{\mathcal{M}^k}, [do(V)]_j)$.

Proof: Recall the generative process (4). Specifically, we are interested in the marginal $p_\theta(\mathbf{V} | [\mathbf{D}^{\mathcal{M}}, do(V)]_j)$. Because of Lemma 1 and Proposition 1 we can write the marginal as a sum over the latents $\mathbf{z}_k \in [\mathbf{z}_j]$ that represent models $\mathcal{M}^k \in [\mathcal{M}^j]$ yielding $\sum_{[\mathbf{z}_j]} p_\gamma(\mathbf{V} | \mathbf{z}_k) p_\eta(\mathbf{z}_k | [\mathbf{D}^{\mathcal{M}}, do(V)]_j)$. Since p_η is a uniform mixture, this is equivalent to $\sum_{[\mathbf{z}_j]} \rho_k p_\gamma(\mathbf{V} | \mathbf{z}_k) = \sum_{\mathcal{M}^k \in [\mathcal{M}^j]} \rho_k p_\theta(\mathbf{V} | \mathbf{D}^{\mathcal{M}^k}, [do(V)]_j)$ since \mathbf{z}_k encodes the model-query pair.

With this, we showed that ACTIVA learns to estimate the causal distribution shift from observational data and a query intervention, up to a mixture of observationally equivalent models. Our predicted distributions explicitly encode uncertainty about the data-generating causal model. Furthermore, these results are, to the best of our knowledge, alongside with results from Balazadeh et al. (2025) on uncertainty quantification in the identifiable data case, among the first steps to build a theory around amortized causal inference. Figure 1 shows the intuition behind our result.

4.1 Practical Considerations

Implementing our theoretical framework (Section 4) in practice involves several approximations. First, directly using Dirac distributions within a VAE framework is impractical due to undefined gradients. We thus approximate Dirac distributions with multivariate normal (MVN) distributions, using a fixed variance and zero covariance, which places each causal model in a distinct region of latent space. The prior is modeled as a Gaussian mixture model (GMM), naturally satisfying Assumption 3 and ensuring mathematical well-definedness of the KL divergence without explicit knowledge of latent locations.

Second, although our decoder (Section 5.4) violates injectivity (Assumption 2), empirical results suggest that this relaxation remains effective. Nonetheless, injective alternatives may offer a better theoretical alignment and represent a promising direction for future work.

Finally, since the prior is a GMM, obtaining closed-form solutions for interventional distributions at inference is intractable. We instead approximate the distribution by sampling 50 latent variables from the prior, decoding them, and constructing a uniform mixture. Despite these relaxations,

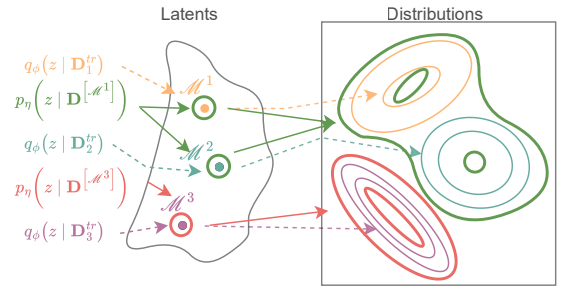


Figure 1: Given observational data $\mathbf{D}^{\mathcal{M}}$ and a query intervention $do(X = x)$, the encoder maps to a latent point and the prior to a mixture of latent points. Samples \mathbf{z} from this latent space are passed to the decoder, which estimates the interventional distribution $p_{\mathcal{M}}(\mathbf{V} | do(X = x))$ as a Gaussian mixture. Dashed lines indicate training-time information flow, solid lines represent inference-time.

our experiments demonstrate robust and practical estimation of interventional distributions.

5 Model Architecture

Our model employs a transformer-based encoder-decoder architecture that estimates interventional distributions from observational data and intervention queries. For detailed hyperparameters, see Appendix C.

5.1 Representing Interventions

To represent interventions, we create a matrix representation of the interventions. We consider $i \in \{1, \dots, |I|\}$ the index of a possible intervention value v_i , where $|I|$ is the number of possible values, and a selector $\mathbf{t} \in \{0, 1\}^d$ indicating the target(s) of the intervention. By not encoding the intervention value directly, but rather the index of the intervention, we remove the need to have a full specification of the intervention. This allows us to model interventional distributions based on placeholder IDs of the interventions, as long as they can be attributed to interventional training data and have specified targets.

We construct the intervention representation $\mathbf{I}_{i,t}$ representing $do(V_t = v_i)$ as follows. We perform a one-hot encoding of i creating a vector $\mathbf{i}_{oh} \in \mathbb{R}^{|I|}$ and repeat it d times, resulting in a matrix $\mathbf{i}_{rep} \in \mathbb{R}^{d \times |I|}$. We then apply \mathbf{t} as a mask to this matrix, effectively zeroing out the rows that correspond to non-intervened variables. Finally, we repeat the intervention representation N times to match the number of input samples and obtain $\mathbf{I}_{i,t} \in \mathbb{R}^{N \times d \times |I|}$.

This construction ensures that the intervention-relevant information for each variable is provided as local information alongside the variable itself and maintains permutation equivariance.

5.2 Embedding Network

We encode the input data and intervention according to an embedding network $h_\alpha(\mathbf{D}^{\mathcal{M}}, \mathbf{I}_{i,t})$ based on the extension

of non-parametric encoders (Kossen et al. 2021; Lorch et al. 2022). For various causal tasks, this architecture can successfully encode a dataset into a vector containing causally relevant information, such as structure (Lorch et al. 2022), topological ordering (Scetbon et al. 2024), informative interventions (Annadani et al. 2025), and effects (Balazadeh et al. 2025; Robertson et al. 2025; Ma et al. 2025).

Given a dataset $\mathbf{D}^{\mathcal{M}} \in \mathbb{R}^{N \times d}$ of N observational samples from a model \mathcal{M} , an intervention index i and a binary target vector \mathbf{t} , we append $\mathbf{I}_{i,t}$ to the dataset resulting in an augmented dataset $\mathbf{D}_{it}^{\mathcal{M}} \in \mathbb{R}^{N \times d \times |I|+1}$. Then we apply L blocks of multi-head self-attention (MHSA) that alternate in attending over d features and N samples. Furthermore, we apply layer normalization, residual connections, and dropout following the transformer setup (Vaswani et al. 2017). After the transformer blocks, we average over the sample axis to obtain an embedding $\mathbf{h} \in \mathbb{R}^{d \times e}$, where e indicates the embedding dimension, thus ensuring that the embedding is permutation invariant regarding the sample dimension and equivariant regarding the feature dimension.

5.3 Prior and Encoder

Following the reasoning in Section 4.1, we choose the conditional prior to be an n -dimensional GMM with constant variance and no covariance whose means, and weights are determined by a learnable prior function $[\mu_{0:d}, \rho_{0:C}] = pri_{\eta}(h_{\alpha'}(\mathbf{D}^{\mathcal{M}}, \mathbf{I}_{i,t}))$. Specifically, pri_{η} are two two-layer multi-layer perceptron (MLP) that we apply to the embedding \mathbf{h}' to each feature independently to compute the means and mixture weights. The outputs parametrize our prior distribution $p_{\eta}(z|\mathbf{D}^{\mathcal{M}}, do(V)) = \sum_{j=0}^{|C|} \rho_j \mathcal{MVN}(z; \mu_j, 0.1^C)$, with μ_j the mean vector of each component, respectively. We enforce $\sum_{j=0}^C \rho_j = 1$ via a softmax layer.

Furthermore, we choose the encoder distribution to be an n -dimensional MVN with constant, diagonal covariance matrix whose means are determined by a learnable encoder function $\mu = enc_{\phi}(h_{\alpha''}(\mathbf{V}, \mathbf{I}_{i,t}), h_{\alpha'}(\mathbf{D}^{\mathcal{M}}, \mathbf{I}_{i,t}))$, where $h_{\alpha'}$ is the observational data network used in the prior, and $h_{\alpha''}$ is the network encoding interventional data with different parameters. We concatenate the resulting embeddings \mathbf{h}' and \mathbf{h}'' along the embedding dimensions and again apply a two-layer MLP to each feature independently to compute the mean. This fully parametrized our encoding distribution $q_{\phi}(z|\mathbf{V}, \mathbf{D}^{\mathcal{M}}, do(V)) = \mathcal{MVN}(z; \mu, 0.1)$.

5.4 Decoder

We model the decoder $dec_{\gamma}(z)$ as a transformer that outputs the parameters of a Gaussian mixture, enabling a closed-form expression for the estimated interventional distributions.

For the decoder we simply process z via K standard transformer blocks (Vaswani et al. 2017) resulting in the embedding \mathbf{h}_{dec} . We feed this embedding through a row-wise linear layer to predict the means $\mu_{\gamma} \in \mathbb{R}^{B \times d}$, where B is the number of decoder mixture components, maintaining permutation equivariance regarding the variable ordering. To

also predict the covariances $\Sigma_{\gamma} \in \mathbb{R}^{B \times d \times d}$ in a permutation equivariant manner, we first apply a row-wise linear layer to compute $\mathbf{u} \in \mathbb{R}^{B \times d \times e}$ as an intermediate step and then compute the covariances via $\mathbf{u} \cdot \mathbf{u}$ similarly to (Lorch et al. 2022). Lastly, we predict the component weights $\mathbf{b}_{0:B}$ of the mixture by first summing \mathbf{h}_{dec} along the d feature dimensions and then passing the pooled representation through a linear layer and a softmax layer.

We note that we maintain permutation equivariance of the means and covariances of the resulting mixture w.r.t. the ordering of the variables end-to-end, a property that has been shown to be important in causal inference for scaling (Lorch et al. 2022) and accuracy (Li, Xiao, and Tian 2020), among others.

6 Experiments

6.1 Datasets

We evaluate the performance of the proposed method across three different types of datasets: two purely synthetic and one semi-synthetic dataset. Below we provide an overview of each dataset category. Detailed information on dataset generation and the exact parameters can be found in A.

Synthetic Data (Gaussian and Beta Noise). We generate data from linear additive causal models of the form $V_j = \sum_{i \in \text{Pa}(j)} \beta_{ij} V_i + \varepsilon_j$, where ε_j is drawn either from a Gaussian distribution $\mathcal{N}(0, \sigma^2)$ or a Beta distribution $\text{Beta}(\alpha, \beta)$. We generate data for single-variable interventions $do(V_i = 5)$ on each variable. In general, linear Gaussian-noise models are not identifiable without additional constraints or interventional data, whereas beta-noise models are identifiable from merely observational data (Peters, Janzing, and Schölkopf 2017), which makes these two model classes interesting for comparison.

Semi-Synthetic (SERGIO). We generate biologically inspired data using the SERGIO simulator (Dibaenia and Sinha 2020) for gene-expression. SERGIO models single-cell gene expressions with the resulting data aligning closely with real gene-expression patterns. Notably, we use the implementation provided by (Lorch et al. 2022) that allows interventions in the simulator. We generate data for single-variable interventions $do(V_i = 0)$ on each variable to simulate gene-knockout.

6.2 Metrics

To assess the fidelity of the learned distributions, we rely on the following three sample-based metrics and a permutation-based statistical test to get a broad picture of the distributional accuracy of our estimations. For all three metrics, lower values are desired. A detailed introduction to these metrics can be found in Appendix B.

Maximum Mean Discrepancy (MMD) (Gretton et al. 2012) is a kernel-based measure that compares the mean embeddings of two distributions. Wasserstein Distance (WSD) (Villani 2009), captures the minimal “transport cost” required to transform one distribution into another. The energy distance (ERG) (Székely and Rizzo 2013) indicates pairwise differences between samples.

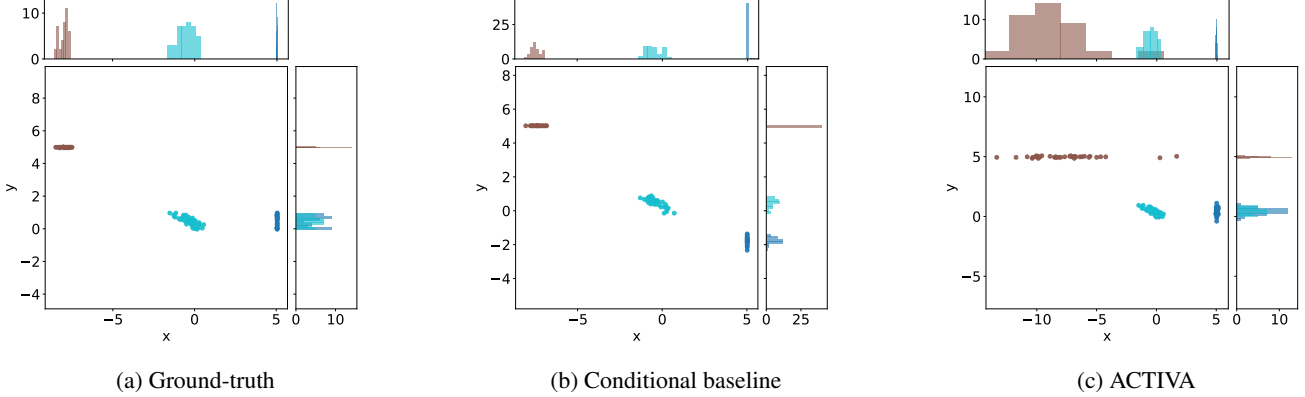


Figure 2: Samples from the observational and interventional distributions of the ground-truth model (a), the conditional baseline (b) and our model (c) for the *Beta* data. The turquoise represent samples from the observational distribution, blue and brown depict samples from the interventional distributions by setting X and Y to 5, respectively. Note that for visualization purposes, we provide the observational samples of the original data for the ACTIVA plot.

Data	ACTIVA			Baseline		
	MMD	WSD	ERG	MMD	WSD	ERG
Gauss 2	0.29	1.9	2.0	0.91	8.0	7.9
Beta 2	0.21	1.4	1.4	0.90	5.8	11.0
Gauss 8	0.65	11.4	12.9	0.88	19.9	16.4
Beta 8	0.77	9.3	13.7	0.94	11.2	19.0

Table 1: Average inference performance of our trained model and the baseline on held-out test data with 2 and 8 variables respectively. The *Data* column indicates which dataset has been used with how many variables.

6.3 Conditional Baseline

We compare with a baseline that estimates the interventional distribution $p(\mathbf{V} \mid \text{do}(\mathbf{V}_t = v_i))$ using conditional distributions. Concretely, it fits a multivariate normal (MVN) to the dataset in order to approximate the observational distribution $p(\mathbf{V})$. From the fitted MVN, it derives the conditional distribution $p(\mathbf{V} \setminus \mathbf{V}_t \mid \mathbf{V}_t = v_i)$. Then, it draws N samples from this conditional distribution and assigns the intervention value v_i to each variable in \mathbf{V}_t . This approach provides a baseline, enabling us to compare the degree to which our method captures genuinely causal information, rather than relying solely on conditioning.

6.4 Distribution Shift Estimation

In this experiment, we examine whether our model’s inference procedure indeed captures causal distribution shifts. Specifically, we train our model on the *Beta* and *Gaussian* datasets, both described in Section 6.1. We first consider the bivariate case where each dataset consists of pairs of variables (X, Y) under distinct causal mechanisms. Next, we extend this evaluation by training ACTIVA on *Gaussian* and *Beta* datasets with 8 variables to show its ability to scale to

more complex scenarios. Details about hyperparameter settings are presented in Appendix C.

Quantitative Analysis. We assess our method’s performance, by comparing it against the conditional baseline on a test set of novel causal models. The models are novel in the sense that while they come from the same distribution of models $p_{tr}(\mathcal{M})$, the models that were sampled in the test set are not in the training set. Table 1 reports the average scores on the two test sets in the bivariate and 8 variable case performing inference with one sample from the prior.

We observe that ACTIVA outperforms the baseline across all metrics and for both model sizes. This validates our implementation of ACTIVA to be able to recover causal distribution shifts beyond conditioning. Furthermore, we observe in the 2 variable case the increased performance on the Beta data compared to the Gaussian data. We interpret this as reflecting the identifiability of the Beta data compared to the general non-identifiability of the Gaussian data. Lastly, we attribute the comparably lower performance margin of the 8 variable models w.r.t. the baseline to non-identifiability in our data (see Assumption 1), as we only provide data with one-variable interventions during training.

Qualitative Analysis. Figure 2 provides a qualitative view of the learned models on the held-out test *Beta* dataset. In this example, there is a negative causal effect from Y to X .

We observe that both the baseline and ACTIVA recover the mean in the causal direction (brown), although ACTIVA has higher uncertainty. More interestingly, the baseline predicts a distribution shift in the anti-causal direction (blue). In contrast, ACTIVA correctly predicts *no* causal effect. Furthermore, it provides a low-probability mode in the causal direction, making uncertainty about the causal model explicit.

Conclusion. These results indicate that our method successfully leverages causal information during inference. By

performing a single forward pass, the model estimates accurate interventional distributions that respect the true causal mechanisms governing the data-generating process.

Data	ACTIVA			Baseline		
	MMD	WSD	ERG	MMD	WSD	ERG
SERGIO	0.34	4.3	1.7	0.50	3.9	2.8
OOD	0.37	7.6	3.7	0.61	8.0	8.0

Table 2: Average inference performance of ACTIVA trained on semi-synthetic data and tested on a held-out test set and an out-of-distribution set.

6.5 Performance on Semi-Synthetic Data

To highlight the potential application of ACTIVA to real scenarios, we employ the *SERGIO* (Dibaeinia and Sinha 2020) simulator for generating gene expression data. Following the setup in (Lorch et al. 2022), we create training and test sets with 8 variables, as well as an out-of-distribution (OOD) evaluation dataset with 11 variables. Appendix A.2 provides a detailed list of the used parameters.

Table 2 compares the baseline to ACTIVA trained on the SERGIO data on the test set and the OOD evaluation set, reporting the average performance metrics. The results largely align with the ones found in Section 6.4, with the exception of almost equal performance on the WSD.

We also observe that performance degrades on the OOD data for both ACTIVA and the baseline. However, in addition to reflecting more challenging conditions, this decrease is partly confounded by the fact that the metrics are sensitive to data scale as detailed in B. Hence, changes in scale between the test (mean value 2.16) and OOD dataset (mean value 3.71) can amplify discrepancies in the reported metrics, even without a reduction in model performance.

Conclusion. ACTIVA exhibits robust performance on unseen semi-synthetic data, confirming its applicability to more realistic domains. Furthermore, ACTIVA remains effective even under distribution shifts, highlighting its potential for handling OOD scenarios. Its advantage over the conditional baseline on semi-synthetic OOD data further highlights the benefits of its causal architecture for estimating interventional distributions and its potential transfer from simulated training data to real-world test data.

7 Related Work

Deep learning approaches to causal inference have advanced modeling of observational, interventional, and counterfactual distributions, yet most demand known or learnable causal graphs and retraining for each new dataset. This holds for variational-autoencoder-based models (Yang et al. 2021; Qi and Yu 2023), diffusion generative models (Sanchez et al. 2022; Chao et al. 2023), graph-neural and flow-based approaches (Zecevi et al. 2021; Sánchez-Martin, Rateike, and Valera 2022; Poinsot et al. 2024), adversarial network approaches (Rahman and Kocaoglu 2024).

Recent amortized estimators leverage prior-fitted networks or supervised learning to predict causal effect distributions without additional training or known causal graphs (Balazadeh et al. 2025; Robertson et al. 2025; Ma et al. 2025). However, they still rely on explicit covariate specification and typically target predefined estimands. Other meta-learning frameworks are restricted to supervised effect estimation (Bynum et al. 2025), enable zero-shot estimation for unseen interventions (Nilforoshan et al. 2023), model the noise as latent (Pawlowski, Castro, and Glocker 2020; De et al. 2023) within the same causal model context, require upfront model assumptions (Löwe et al. 2022) and graphs (Mahajan et al. 2024).

Joint inference methods that jointly learn graphs and mechanisms likewise require dataset-specific optimisation (Lorch et al. 2021; Nishikawa-Toomey et al. 2022; Deleu et al. 2023). Other approaches focus on estimating treatment-outcome relationships without modeling the whole distribution (Louizos et al. 2017; Vowels, Cihan Camgoz, and Bowden 2021; Wu and Fukumizu 2023), require dataset-specific retraining (Khemakhem et al. 2021; Melnychuk, Frauen, and Feuerriegel 2023) or are limited to specific classes of causal models (Cundy, Grover, and Ermon 2021). Some approaches focus on special cases, such as limited overlap or marginal interventional data, but cannot handle joint distributions across all variables (Vanderschueren et al. 2023; Garrido et al. 2024).

In contrast, our method amortizes across both causal structures and mechanisms, requiring only observational data and a specified intervention to return the full joint interventional distribution in a single forward pass. It therefore removes the need for retraining, covariate decomposition, or graphical assumptions.

8 Conclusion

We introduce ACTIVA, a VAE architecture for amortized causal distribution estimation. During training, the encoder maps interventional data — conditioned on observational inputs and a query intervention — to a latent representation, and the decoder reconstructs the corresponding interventional distribution. At inference time, conditioning solely on observational data yields a prior over plausible causal models, which the decoder transforms into a mixture of model-specific interventional distributions. We provide a rigorous theoretical analysis of these latent and output spaces and empirically validate our implementation on synthetic and semi-synthetic datasets. ACTIVA’s primary strengths include its capability for zero-shot inference using observational data alone. This work is among the first works that offer a theoretical foundation for amortized causal inference.

Future work will focus on bridging the gap between theoretical assumptions and implementation, thoroughly evaluating ACTIVA’s performance on real-world datasets to better understand the simulation-to-reality transfer, and exploring alternative deep learning architectures aligned with the developing theory of amortized causal inference. We hope this work inspires further developments in rethinking causal inference in an amortized learning context with both theoretical and practical advances.

Acknowledgments We thank Frank van Harmelen, Emile van Krieken, Majid Mohammadi and Álvaro Serra-Gómez for their helpful inputs to this project.

This research was partially funded by the Hybrid Intelligence Center, a 10-year programme funded by the Dutch Ministry of Education, Culture and Science through the Netherlands Organisation for Scientific Research, <https://hybrid-intelligence-centre.nl>, grant number 024.004.022

References

Annadani, Y.; Tigas, P.; Bauer, S.; and Foster, A. 2025. Amortized Active Causal Induction with Deep Reinforcement Learning. *Advances in Neural Information Processing Systems*, 37: 44216–44239.

Bal, H.; Epema, D.; de Laat, C.; van Nieuwpoort, R.; Romein, J.; Seinstra, F.; Snoek, C.; and Wijshoff, H. 2016. A Medium-Scale Distributed System for Computer Science Research: Infrastructure for the Long Term. *Computer*, 49(5): 54–63.

Balazadeh, V.; Kamkari, H.; Thomas, V.; Li, B.; Ma, J.; Cresswell, J. C.; and Krishnan, R. G. 2025. CausalPFN: Amortized Causal Effect Estimation via In-Context Learning. *arXiv preprint*.

Bareinboim, E.; Correa, J. D.; Ibeling, D.; and Icard, T. 2022. On Pearl’s Hierarchy and the Foundations of Causal Inference. *Probabilistic and Causal Inference*, 507–556.

Bradbury, J.; Frostig, R.; Hawkins, P.; Johnson, M. J.; Leary, C.; Maclaurin, D.; Necula, G.; Paszke, A.; VanderPlas, J.; Wanderman-Milne, S.; and Zhang, Q. 2018. JAX: composable transformations of Python+NumPy programs.

Bynum, L. E. J.; Puli, A.; Herrero-Quevedo, D.; Nguyen, N.; Fernandez-Granda, C.; Cho, K.; and Ranganath, R. 2025. Black Box Causal Inference: Effect Estimation via Meta Prediction. *arXiv preprint*.

Chao, P.; Blöbaum, P.; Prasad, S.; and Amazon, K. 2023. Interventional and Counterfactual Inference with Diffusion Models. *arXiv preprint*.

Cundy, C.; Grover, A.; and Ermon, S. 2021. BCD Nets: Scalable Variational Approaches for Bayesian Causal Discovery. *Advances in Neural Information Processing Systems*, 34: 7095–7110.

De, F.; Ribeiro, S.; Xia, T.; Monteiro, M.; Pawłowski, N.; and Glockner, B. 2023. High Fidelity Image Counterfactuals with Probabilistic Causal Models. In *arXiv preprint*. ISBN 2306.15764v2.

Deleu, T.; Nishikawa-Toomey, M.; Subramanian, J.; Malkin, N.; Charlin, L.; and Bengio, Y. 2023. Joint Bayesian Inference of Graphical Structure and Parameters with a Single Generative Flow Network. In Oh, A.; Neumann, T.; Globerson, A.; Saenko, K.; Hardt, M.; and Levine, S., eds., *Advances in Neural Information Processing Systems*, volume 36, 31204–31231. Curran Associates, Inc.

Dibaeinia, P.; and Sinha, S. 2020. SERGIO: A Single-Cell Expression Simulator Guided by Gene Regulatory Networks. *Cell Systems*, 11(3): 252–271.

Dozat, T. 2016. Incorporating Nesterov Momentum into Adam.

Erdős, P.; and Rényi, A. 1959. On random graphs. *Publicationes Mathematicae*, 290–297.

Garreau, D.; Jitkrittum, W.; and Kanagawa, M. 2017. Large sample analysis of the median heuristic. *arXiv preprint*.

Garrido, S.; Kirschbaum, E.; Kekic, A.; and Mastakouri, A. 2024. Estimating Joint interventional distributions from marginal interventional data. *arXiv preprint*.

Gretton, A.; Borgwardt, K. M.; Rasch, M. J.; Smola, A.; Schölkopf, B.; and Smola GRETTON, A. 2012. A Kernel Two-Sample Test. *Journal of Machine Learning Research*, 13(25): 723–773.

Heek, J.; Levskaya, A.; Oliver, A.; Ritter, M.; Rondepierre, B.; Steiner, A.; and van Zee, M. 2024. Flax: A neural network library and ecosystem for JAX.

Higgins, I.; Matthey, L.; Pal, A.; Burgess, C.; Glorot, X.; Botvinick, M.; Mohamed, S.; and Lerchner, A. 2017. beta-VAE: Learning Basic Visual Concepts with a Constrained Variational Framework. In *International conference on learning representations*.

Hoffman, M. D.; and Johnson, M. 2016. ELBO surgery: yet another way to carve up the variational evidence lower bound. In *Workshop in Advances in Approximate Bayesian Inference NIPS*.

Khemakhem, I.; Monti, R. P.; Leech, R.; and Hyvärinen, A. 2021. Causal Autoregressive Flows. In *International conference on artificial intelligence and statistics*, volume 130, 3520–3528. PMLR.

Kingma, D. P.; and Welling, M. 2013. Auto-Encoding Variational Bayes. *2nd International Conference on Learning Representations, ICLR 2014 - Conference Track Proceedings*.

Kosken, J.; Band, N.; Lyle, C.; Gomez, A. N.; Rainforth, T.; and Gal, Y. 2021. Self-Attention Between Datapoints: Going Beyond Individual Input-Output Pairs in Deep Learning. *Advances in Neural Information Processing Systems*, 34: 28742–28756.

Kumar, S.; Vivek, Y.; Ravi, V.; and Bose, I. 2023. Causal Inference for Banking Finance and Insurance A Survey. *arXiv preprint*.

Li, H.; Xiao, Q.; and Tian, J. 2020. Supervised Whole DAG Causal Discovery. *arXiv preprint*.

Lorch, L.; Rothfuss, J.; Schölkopf, B.; and Krause, A. 2021. DiBS: Differentiable Bayesian Structure Learning. *Advances in Neural Information Processing Systems*, 34: 24111–24123.

Lorch, L.; Sussex, S.; Rothfuss, J.; Krause, A.; and Schölkopf, B. 2022. Amortized Inference for Causal Structure Learning. In Koyejo, S.; Mohamed, S.; Agarwal, A.; Belgrave, D.; Cho, K.; and Oh, A., eds., *Advances in Neural Information Processing Systems*, volume 35, 13104–13118. Curran Associates, Inc.

Louizos, C.; Shalit, U.; Mooij, J. M.; Sontag, D.; Zemel, R.; and Welling, M. 2017. Causal Effect Inference with Deep

Latent-Variable Models. *Advances in Neural Information Processing Systems*, 30.

Löwe, S.; Madras, D.; Zemel, R.; and Welling, M. 2022. Amortized Causal Discovery: Learning to Infer Causal Graphs from Time-Series Data. In Schölkopf, B.; Uhler, C.; and Zhang, K., eds., *Proceedings of the First Conference on Causal Learning and Reasoning*, volume 177 of *Proceedings of Machine Learning Research*, 509–525. PMLR.

Ma, Y.; Frauen, D.; Javurek, E.; and Feuerriegel, S. 2025. Foundation Models for Causal Inference via Prior-Data Fitted Networks. *arXiv preprint*.

Maathuis, M. H.; Kalisch, M.; Bühlmann, P.; and Zürich, E. 2009. Estimating High-Dimensional Intervention Effects from Observational Data. *The Annals of Statistics*, 37(6A): 3133–3164.

Mahajan, D.; Gladrow, J.; Hilmkil, A.; Zhang, C.; and Scetbon, M. 2024. Zero-Shot Learning of Causal Models. *arXiv preprint*.

Marbach, D.; Schaffter, T.; Mattiussi, C.; and Floreano, D. 2009. Generating realistic in silico gene networks for performance assessment of reverse engineering methods. *Journal of computational biology : a journal of computational molecular cell biology*, 16(2): 229–239.

Melnichuk, V.; Frauen, D.; and Feuerriegel, S. 2023. Normalizing Flows for Interventional Density Estimation. In *International Conference on Machine Learning*, 24361–24397.

Montagna, F.; Cairney-Leeming, M.; Sridhar, D.; and Locatello, F. 2024. Demystifying amortized causal discovery with transformers. *arXiv preprint*.

Nilforoshan, H.; Moor, M.; Roohani, Y.; Chen, Y.; Šurina, A.; Yasunaga, M.; Oblak, S.; and Leskovec, J. 2023. Zero-shot causal learning. In *Advances in Neural Information Processing Systems*.

Nishikawa-Toomey, M.; Deleu, T.; Subramanian, J.; Bengio, Y.; and Charlin, L. 2022. Bayesian learning of Causal Structure and Mechanisms with GFlowNets and Variational Bayes. *arXiv preprint*.

Panizza, U.; and Presbitero, A. F. 2014. Public debt and economic growth: Is there a causal effect? *Journal of Macroeconomics*, 41: 21–41.

Pawlowski, N.; Castro, D. C.; and Glockner, B. 2020. Deep Structural Causal Models for Tractable Counterfactual Inference. In *Advances in neural information processing systems*, 857–869.

Peters, J.; Janzig, D.; and Schölkopf, B. 2017. *Elements of causal inference: foundations and learning algorithms*. The MIT Press.

Poinsot, A.; Leite, A.; Chesneau, N.; Sébag, M.; and Schönenauer, M. 2024. Learning Structural Causal Models through Deep Generative Models: Methods, Guarantees, and Challenges. *arXiv preprint*.

Qi, G.; and Yu, H. 2023. CMVAE: Causal Meta VAE for Unsupervised Meta-Learning. *Proceedings of the AAAI Conference on Artificial Intelligence*, 37(8): 9480–9488.

Rahman, M. M.; and Kocaoglu, M. 2024. Modular Learning of Deep Causal Generative Models for High-dimensional Causal Inference. *arXiv preprint*.

Robertson, J.; Reuter, A.; Guo, S.; Hollmann, N.; †4, F. H.; and Schölkopf, B. 2025. Do-PFN: In-Context Learning for Causal Effect Estimation. *arXiv preprint*.

Sanchez, P.; Tsafaris, S. A.; Schölkopf, B.; Uhler, C.; and Zhang, K. 2022. Diffusion Causal Models for Counterfactual Estimation.

Sánchez-Martin, P.; Rateike, M.; and Valera, I. 2022. VACA: Designing Variational Graph Autoencoders for Causal Queries. *Proceedings of the AAAI Conference on Artificial Intelligence*, 36(7): 8159–8168.

Sauter, A.; Acar, E.; and Plaat, A. 2024. CausalPlayground: Addressing Data-Generation Requirements in Cutting-Edge Causality Research. *arXiv preprint*.

Sauter, A. W. M.; Botteghi, N.; Acar, E.; and Plaat, A. 2024. CORE: Towards Scalable and Efficient Causal Discovery with Reinforcement Learning. *Proceedings of the 23rd International Conference on Autonomous Agents and Multiagent Systems (AAMAS)*, 1664–1672.

Scetbon, M.; Jennings, J.; Hilmkil, A.; Zhang, C.; and Ma, C. 2024. A Fixed-Point Approach for Causal Generative Modeling.

Shi, J.; and Norgeot, B. 2022. Learning Causal Effects From Observational Data in Healthcare: A Review and Summary. *Frontiers in Medicine*, 9: 864882.

Sohn, K.; Yan, X.; and Lee, H. 2015. Learning Structured Output Representation using Deep Conditional Generative Models. *Advances in Neural Information Processing Systems*.

Székely, G. J.; and Rizzo, M. L. 2013. Energy statistics: A class of statistics based on distances. *Journal of Statistical Planning and Inference*, 143(8): 1249–1272.

Vanderschueren, T.; Berrevoets, J.; Verbeke, W.; and Leuven, K. U. 2023. NOFLITE: Learning to Predict Individual Treatment Effect Distributions. *Transactions on Machine Learning Research*.

Vaswani, A.; Vaswani, A.; Shazeer, N.; Parmar, N.; Uszkoreit, J.; Jones, L.; Gomez, A. N.; Kaiser, L.; and Polosukhin, I. 2017. Attention Is All You Need. In *Advances in Neural Information Processing Systems*.

Villani, C. 2009. *Optimal Transport*, volume 338 of *Grundlehren der mathematischen Wissenschaften*. Berlin, Heidelberg: Springer Berlin Heidelberg. ISBN 978-3-540-71049-3.

Vowels, M. J.; Cihan Camgoz, N.; and Bowden, R. 2021. Targeted VAE: Variational and Targeted Learning for Causal Inference. *IEEE International Conference on Smart Data Services*.

Wu, P.; and Fukumizu, K. 2023. β -Intact-VAE: Identifying and Estimating Causal Effects under Limited Overlap. *International Conference on Learning Representation*.

Yang, M.; Liu, F.; Chen, Z.; Shen, X.; Hao, J.; and Wang, J. 2021. CausalVAE: Disentangled Representation Learning via Neural Structural Causal Models. *Proceedings of*

the IEEE/CVF Conference on Computer Vision and Pattern Recognition (CVPR).

Zečevi, M.; Singh Dhami, D.; Veličkovi, P.; and Kersting KERSTING, K. 2021. Relating Graph Neural Networks to Structural Causal Models. *arXiv preprint*.

parameter	in-distribution	out-of-distribution
genes	8	11
b	Uniform(0, 1)	Uniform(0.5, 2.0)
k_param	Uniform(1, 5)	Uniform(3, 7)
k_sign	Beta(1, 1)	Beta(0.5, 0.5)
hill	$\in \{1.9, 2.0, 2.1\}$	$\in \{1.5, 2.5\}$
decays	$\in \{0.7, 0.8, 0.9\}$	$\in \{0.5, 1.5\}$
noise_params	$\in \{0.9, 1.0, 1.1\}$	$\in \{0.5, 1.5\}$

Table 3: Caption

A Datasets

We evaluate the performance of the proposed method across three different types of datasets: two purely synthetic (*Gaussian* and *Beta*) and one semi-synthetic (*SERGIO*). Below, we provide an overview of each dataset category along with the relevant parameters. For every causal model in these categories, we draw N samples from both the observational and the interventional distributions to create paired datasets. Details about the exact number of models, how we split into training/test sets, and further parameter choices are given in the subsections below.

A.1 Synthetic Data (Gaussian and Beta Noise)

We generate data from linear additive causal models of the form:

$$V_j = \sum_{i \in \text{Pa}(j)} \beta_{ij} V_i + \varepsilon_j,$$

where ε_j is drawn from either: A Gaussian distribution, $\mathcal{N}(0, \sigma^2)$, or A Beta distribution, $\text{Beta}(\alpha, \beta)$. For each variable V_i , we generate interventional data by applying a single-variable intervention $\text{do}(V_i = 5)$ plus some noise $\mathcal{N}(0, 0.1)$ to increase numerical stability. In total, this yields one observational dataset and d interventional dataset for each causal model. All synthetic data is generated with the *Causal Playground* library (Sauter, Acar, and Plaat 2024).

The causal graphs are generated according to the ER procedure (Erdős and Rényi 1959) where first we generate an ER graph with edge-probability 0.3 and then randomly remove edges until the graph becomes acyclic. When the noise terms follow a Gaussian distribution, we sample β_{ij} uniformly from $[-2, -0.5] \cup [0.5, 2]$ and let $\varepsilon_j \sim \mathcal{N}(0, 0.5^2)$. For the Beta case, we again draw β_{ij} in $[-2, -0.5] \cup [0.5, 2]$, but the noise terms ε_j follow $\text{Beta}(\alpha, \beta)$ with $\alpha, \beta \sim \text{Uniform}(0.5, 2)$.

We examine both a 2-variable and an 8-variable scenario:

- **Two Variables.** We randomly generate 10000 linear models and sample 40 points each for the observational and interventional distributions. We split these 10000 models into 9000 for training and 1000 for testing.
- **Eight Variables.** We generate 30000 linear models. For each model, we sample 30 data points for the observational and for each interventional distribution. Of these 30000 models, 27000 are used for training and 3000 are held out for testing.

A.2 Semi-Synthetic Data (SERGIO)

To evaluate on data with biological realism, we employ the SERGIO simulator (Dibaeinia and Sinha 2020), which generates single-cell gene-expression data. Notably, we use the version of SERGIO provided in (Lorch et al. 2022), which includes functionality for performing interventions. We treat single-gene knockouts as interventions, thus applying $\text{do}(V_i = 0)$ to each gene V_i . This yields one observational dataset and 8 single-gene interventional datasets per simulated gene-regulatory network.

Simulator Settings and Network Structures. Following the procedure in (Marbach et al. 2009; Lorch et al. 2021), we randomly sample subgraphs of known gene-regulatory networks from *E. coli* or *S. cerevisiae*, ensuring that each subgraph has 8 genes. For each subgraph, we draw model parameters (e.g., activation constants, decay rates, and noise magnitudes) from predefined ranges (Table 3). We then generate observational data as well as data from each gene-knockout intervention.

Training, Testing, and Out-of-Distribution (OOD) Splits. We run 15,000 SERGIO simulations for our in-distribution dataset and sample 30 cells (data points) for each observational and interventional condition. We then split these 15,000 simulations into training (90%) and test (10%). We also construct an OOD set of 1800 simulations, where some SERGIO parameters (e.g., noise or decay rates) are sampled from partially disjoint ranges, creating a controlled distribution shift. For evaluation, we again sample 30 cells per observational/interventional condition in these OOD simulations.

In summary, the synthetic datasets allow us to systematically analyze the ability of our amortized approach to capture linear causal effects under distinct noise assumptions, while the semi-synthetic SERGIO datasets bring our method closer to real-world conditions by simulating biologically realistic gene-expression data under interventions.

B Metrics

To quantitatively assess how closely our estimated interventional distributions align with the ground-truth or observed distributions, we employ three sample-based distance measures and a permutation-based statistical test. Specifically, we use:

- **Maximum Mean Discrepancy (MMD)**
- **Wasserstein Distance (WSD)**
- **Energy Distance (ERG)**

Each of these distances captures a distinct notion of distributional similarity. The MMD is a kernel-based embedding measure that detects differences in distribution means in a reproducing kernel Hilbert space; the Wasserstein distance considers a geometric “transport cost” viewpoint; and the energy distance focuses on pairwise distance comparisons. Taken together, these three metrics give a robust picture of how well our learned distributions match the ground truth in terms of shape, location, and higher-order moments.

Maximum Mean Discrepancy (MMD). The MMD (Gretton et al. 2012) compares the mean embeddings of two distributions, P and Q , in a reproducing kernel Hilbert space (RKHS). Concretely, for samples $\{\mathbf{x}_i\}_{i=1}^m \sim P$ and $\{\mathbf{y}_j\}_{j=1}^n \sim Q$, MMD is computed as:

$$\text{MMD}^2(P, Q) = \mathbb{E}_{\mathbf{x}, \mathbf{x}' \sim P}[k(\mathbf{x}, \mathbf{x}')] + \mathbb{E}_{\mathbf{y}, \mathbf{y}' \sim Q}[k(\mathbf{y}, \mathbf{y}')] - 2\mathbb{E}_{\mathbf{x} \sim P, \mathbf{y} \sim Q}[k(\mathbf{x}, \mathbf{y})],$$

where $k(\cdot, \cdot)$ is a positive-definite kernel. Lower MMD values indicate that the two sets of samples are more similar with respect to that kernel-induced feature map. In our experiments, we use a Gaussian (RBF) kernel

$$k_\sigma(\mathbf{x}, \mathbf{y}) = \exp\left(-\frac{\|\mathbf{x} - \mathbf{y}\|^2}{2\sigma^2}\right),$$

whose bandwidth parameter σ is chosen via the median heuristic (i.e., by setting the kernel scale to the median distance among all pairs of training samples). This approach is a common, adaptive way to select an appropriate kernel width without extensive hyperparameter tuning (Garreau, Jitkrittum, and Kanagawa 2017).

Wasserstein Distance (WSD). Also referred to as the Earth Mover’s Distance, the Wasserstein distance (Villani 2009) evaluates how much “effort” is needed to transform one distribution into another. Formally, for $p \geq 1$:

$$\mathcal{W}_p(P, Q) = \left(\inf_{\gamma \in \Gamma(P, Q)} \int_{\mathcal{X} \times \mathcal{X}} d(\mathbf{x}, \mathbf{y})^p d\gamma(\mathbf{x}, \mathbf{y}) \right)^{1/p},$$

where $\Gamma(P, Q)$ is the set of all couplings of P and Q , and $d(\mathbf{x}, \mathbf{y})$ is a distance metric (usually Euclidean). A lower Wasserstein distance indicates that the two distributions are closer in a geometric sense, reflecting both differences in location and in spread.

Energy Distance (ERG). The energy distance (Szekely and Rizzo 2013) offers yet another perspective on distributional similarity by comparing pairwise distances:

$$\text{ED}(P, Q) = \mathbb{E}[\|\mathbf{X} - \mathbf{Y}\|] - \frac{1}{2}\mathbb{E}[\|\mathbf{X} - \mathbf{X}'\|] - \frac{1}{2}\mathbb{E}[\|\mathbf{Y} - \mathbf{Y}'\|],$$

where $\mathbf{X}, \mathbf{X}' \sim P$ and $\mathbf{Y}, \mathbf{Y}' \sim Q$. Lower energy distance values indicate higher overall similarity between P and Q in terms of both mean locations and dispersion patterns.

Energy-Based Permutation Test. Finally, we apply a permutation test based on the energy distance to determine whether two sets of samples are statistically indistinguishable from one another. Specifically, we first compute the observed energy distance D_{obs} between the real (or ground-truth) samples and the model-generated samples. Then we pool the two sets of samples and repeatedly sample 100 random permutations to split them into two groups of the original sizes. Finally we compute the energy distance D_{perm} for each permutation, thereby approximating a null distribution in which P and Q are “mixed.”

If D_{obs} is not significantly larger than typical D_{perm} values (at a chosen significance level), we fail to reject the null hypothesis that both sets of samples come from the same distribution. Hence, a high p -value indicates that our learned samples are statistically indistinguishable from the ground truth.

C Hyperparameters

Table 4 provides a summary of the principal hyperparameters used in our experiments, along with their chosen values for each model variant.

Models and Experiments.

- *Gauss 2* and *Beta 2* refer to the models used in the bivariate experiments described in 6.4.
- *Gauss 8* and *Beta 8* analogously represent versions for the eight-variable models.
- *SERGIO* is the version of our model employed for the semi-synthetic gene-expression data of the experiment in 6.5).

Explanation of Table Columns.

- **Batch size** indicates how many datasets are processed in each training step.
- **Heads** is the number of heads used in the multi-head self-attention layers.
- **K** (in our table notation) specifies the number of Transformer blocks used in the decoder.
- **L** is the number of Transformer blocks in the encoder, alternating attention over sample and feature axes. This always has to be an even number.
- **Dropout** is the probability of randomly dropping units in the attention and feed-forward sublayers.
- **e** indicates the embedding dimension for each feature before attention is applied.
- **h** hidden dimension of the neural networks throughout the model.
- **d** is the dimensionality of input features.
- **c** denotes the number of Gaussian components used in the mixture for the decoder’s output distribution.
- **k** denotes the number of Gaussian components used in the mixture for the prior distribution.
- **epochs** is the total number of passes through the training dataset.
- **lr** is the learning rate used for the Adam-based optimizer (Dozat 2016).
- **seed** ensures reproducibility of parameter initialization and dataset splits.
- β is the coefficient that balances the KL term in our β -VAE training objective (see Section 4 of the main text). A value less than 1 places more emphasis on accurate reconstruction over disentanglement.
- **GPU** on which the model was trained.

	batch size	heads	K	dropout	e	h	d	c	k	L	epochs	lr	seed	β	GPU
Gauss 2	256	2	4	0.1	64	128	2	1	2	2	5000	0.001	42	0.1	A6000
Beta 2	256	2	4	0.1	64	128	2	1	2	2	5000	0.001	42	0.1	A6000
Gauss 8	256	4	4	0.1	64	512	2	1	2	4	3600	0.0005	42	0.1	A6000
Beta 8	256	4	4	0.1	64	512	2	1	2	4	3600	0.0005	42	0.1	A6000
SERGIO	256	4	4	0.1	64	256	2	1	2	4	4100	0.0005	42	0.1	A100

Table 4: Hyperparameter configurations for the main experiments. Each row represents one of our trained models, indicating how it was set up in terms of architecture depth, dimensionality, and optimization parameters.

Training times vary depending on model size (d, e, c) and dataset size (batch size, epochs). Larger mixture components (c) and higher embedding dimensions (e) generally increase both training time and representational capacity. Potential NaN’s in the optimization are zeroed. All modules and training scripts were implemented with Jax (Bradbury et al. 2018) and Flax (Heek et al. 2024). Experiment were run on the DAS6 computing cluster (Bal et al. 2016).

In summary, the hyperparameters in Table 4 reflect our balancing of model complexity, regularization, and computational resource constraints. Values are chosen empirically to ensure stable training and satisfactory performance across different experimental settings.